

Validating first-principles phonon lifetimes via inelastic neutron scattering

Enda Xiao ^{1,*}, Hao Ma ^{2,*}, Matthew S. Bryan ^{2,*}, Lyuwen Fu ³, J. Matthew Mann,⁴ Barry Winn,⁵ Douglas L. Abernathy ⁵, Raphaël P. Hermann ², Amey R. Khanolkar,⁶ Cody A. Dennett ⁶, David H. Hurley ⁶, Michael E. Manley ² and Chris A. Marianetti ³

¹*Department of Chemistry, Columbia University, New York, New York 10027, USA*

²*Materials Science and Technology Division, Oak Ridge National Laboratory, Oak Ridge, Tennessee 37831, USA*

³*Department of Applied Physics and Applied Mathematics, Columbia University, New York, New York 10027, USA*

⁴*Air Force Research Laboratory, Sensors Directorate, Wright-Patterson Air Force Base, Ohio 45433, USA*

⁵*Neutron Scattering Division, Oak Ridge National Laboratory, Oak Ridge, Tennessee 37831, USA*

⁶*Materials Science and Engineering Department, Idaho National Laboratory, Idaho Falls, Idaho 83415, USA*



(Received 22 February 2022; revised 3 August 2022; accepted 5 October 2022; published 24 October 2022)

Phonon lifetimes are a key component of quasiparticle theories of transport; yet first-principles lifetimes are rarely directly compared with inelastic neutron scattering (INS) results. Existing comparisons show discrepancies even at temperatures where perturbation theory is expected to be reliable. In this paper, we demonstrate that the reciprocal space voxel (q voxel), which is the finite region in reciprocal space required in INS data analysis, must be explicitly accounted for within theory in order to draw a meaningful comparison. We demonstrate accurate predictions of peak widths of the scattering function when accounting for the q voxel in CaF_2 and ThO_2 . Passing this test implies high fidelity of the phonon interactions and the approximations used to compute the Green's function, serving as a critical benchmark of theory and indicating that other material properties should be accurately predicted, which we demonstrate for thermal conductivity.

DOI: [10.1103/PhysRevB.106.144310](https://doi.org/10.1103/PhysRevB.106.144310)

When computing anharmonic vibrational properties from first principles, various approximations are employed, making it challenging to assess the integrity of any single observable as compared with experiment (e.g., thermal conductivity). Comparing a q -space-resolved observable (e.g., the scattering function) inherently provides a large number of comparisons, offering a very stringent test. While verification of the harmonic vibrational first-principles Hamiltonian is a standard practice, the same cannot be said for the anharmonic vibrational Hamiltonian and subsequent approximations which are used to compute observables. Anharmonic terms result in finite phonon lifetimes yielding finite widths of the peaks in the scattering function. A direct comparison of peak width between theory and inelastic neutron scattering (INS) is rare, and existing studies reveal anomalous discrepancies. A recent study on Si notes the large discrepancy between theory and experiment, leading the authors to only compare the relative change as a function of temperature [1]. A study on Al at high temperatures finds that perturbation theory does not reliably predict the experimental peak width, and their first-principles molecular dynamics simulations often differ from experiment by a factor of 2 [2].

Here we show that a proper comparison between the theoretical scattering function and the experimental scattering function requires an explicit accounting for the finite region probed in reciprocal space, which is referred to as the q voxel. Due to the flux-limited nature of INS, there is a minimum

region of q space which can be sampled while maintaining sufficient statistics, and therefore there is a minimum q -voxel size below which INS cannot probe. Depending on the measurement type, the q -voxel shape is either set by the instrument configuration (for triple-axis measurements) or defined postmeasurement in the analysis of large volumes of data (for time-of-flight measurements). This work will focus on the latter since the large data volumes allow for a more comprehensive assessment across many zones and with varying q voxels. While there is no formal standard for choosing a q voxel, it is typical to choose the q -voxel size and shape based on the shape of the phonon dispersion surface, selecting a smaller dimension along directions with steeper dispersion and larger dimensions along directions with flatter dispersion.

In this paper, we demonstrate the critical role of the q voxel using two fluorite structured materials, ThO_2 and CaF_2 , showing excellent agreement between peak widths within a q voxel obtained from INS and computed from perturbation theory based on the first-principles phonons and cubic phonon interactions. Successful agreement validates both the anharmonic Hamiltonian and the level of theory being used to evaluate the scattering function. Given our successful peak-width predictions, it is expected that thermal conductivity predicted using the same anharmonic Hamiltonian and the Boltzmann transport equation should faithfully describe experimental measurements in some temperature regime, which is demonstrated for CaF_2 and ThO_2 .

Time-of-flight INS measurements were performed using the Wide-Angular-Range Chopper Spectrometer (ARCS) [3] and Hybrid Spectrometer (HYSPEC) [4] instruments

*These authors contributed equally to this work.

at the Spallation Neutron Source. Thermal conductivity measurements were made on single-crystal ThO_2 using spatial domain thermoreflectance (SDTR) via the methods described in Ref. [5]. First-principles calculations were performed using density functional theory (DFT) with the strongly constrained and appropriately normed (SCAN) functional [6], and phonons and cubic phonon interactions were computed using the lone and bundled irreducible derivative approaches [7,8]. Detailed information about experimental and computational methods is included in the Supplemental Material [8].

In order to compute the phonon linewidths and the one-phonon scattering function $S_1(\mathbf{Q}, \omega)$, the single-particle phonon Green's function can be approximately evaluated using the phonons and cubic phonon interactions within leading-order perturbation theory [9,10] (see Eq. (2) in the Supplemental Material [8]). The scattering function $S_1(\mathbf{Q}, \omega)$ is evaluated precisely at \mathbf{Q} , but in INS experiments a finite q voxel must be chosen to provide sufficient counting statistics. This q voxel can be accounted for theoretically by integrating $S_1(\mathbf{Q}, \omega)$ over the q voxel, resulting in

$$S_1^{\text{vox}}(\mathbf{Q}, \omega) = \frac{1}{\Omega_{\text{vox}}} \int_{\text{vox}} d^3Q' S_1(\mathbf{Q}', \omega), \quad (1)$$

where Ω_{vox} is the reciprocal space volume of the q voxel. For clarity, we refer to $S_1(\mathbf{Q}, \omega)$ as the q -point scattering function and $S_1^{\text{vox}}(\mathbf{Q}, \omega)$ as the q -voxel scattering function. It should be noted that the widths of $S_1^{\text{vox}}(\mathbf{Q}, \omega)$ can vary from zone to zone, unlike $S_1(\mathbf{Q}, \omega)$ [8].

We now proceed to evaluate the q -point and q -voxel scattering functions in CaF_2 and ThO_2 and compare them with INS measurements. Given that CaF_2 and ThO_2 are band insulators, standard implementations of DFT are expected to perform well in terms of describing the ground-state properties. As anticipated, the computed phonon spectrum is in good agreement with the scattering function peak positions obtained from INS at ambient temperature for both CaF_2 [see Fig. 1(a)] and ThO_2 (see Fig. S2 in the Supplemental Material [8]). While the peak locations agree well, it is interesting to directly compare the respective scattering functions via contour plots along a path through q space [see Fig. 1(b)]. For a direct comparison, the INS instrumental energy resolution is accounted for in the theoretical result [3]. We find that the theoretical and INS q -voxel scattering functions are in reasonable agreement, while they have nontrivial differences with the q -point scattering function in certain regions. The theoretical q -voxel scattering function even recovers subtle features of the INS, such as the presence of the TA-1 band [see Fig. 1(a) for naming convention], which is forbidden in the q -point scattering function for the path shown but is visible in the q -voxel scattering function [11]. In order to illustrate potential differences between the q -point and q -voxel scattering functions, both large and small, we present the scattering function at two Q points as a function of energy around the LO1 band, which scatters strongly [see Figs. 1(c) and 1(d)]. As shown, the Q which is closer to the zone center [Fig. 1(d)] only shows negligible differences between the q -point and q -voxel scattering functions, while the other Q [Fig. 1(c)] shows good agreement between the theoretical and experimental q -voxel scattering functions, but a substantial difference with the q -point scattering function; and this difference may be attributed

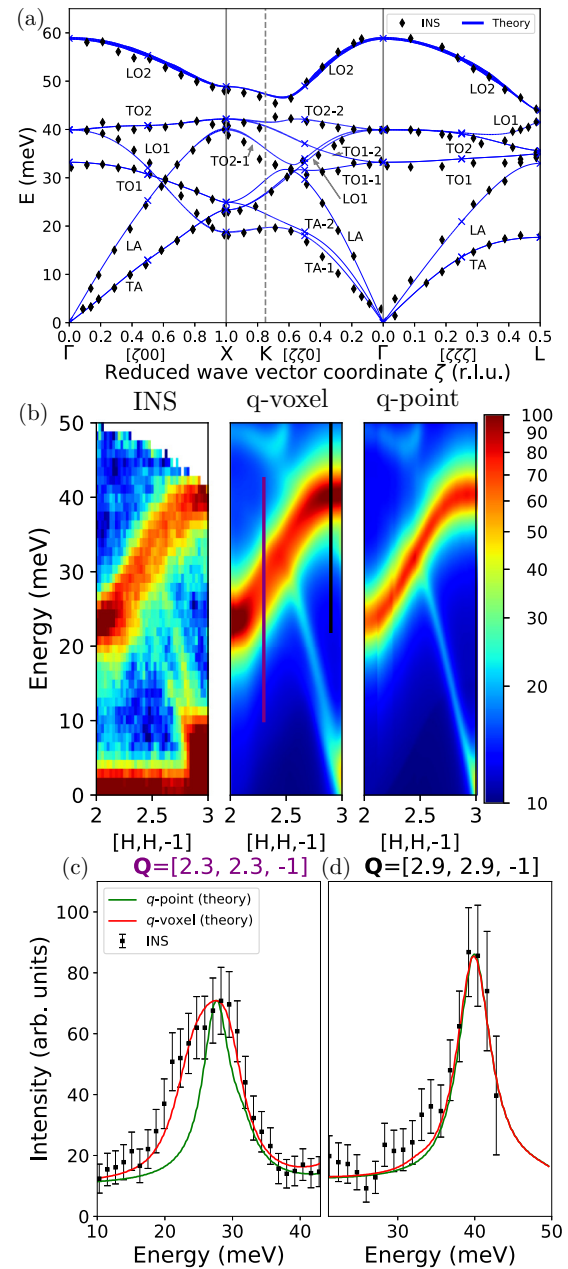


FIG. 1. (a) Phonon dispersion of CaF_2 . Black points are INS measurements at $T = 300$ K; blue crosses are computed using DFT (SCAN), blue curves are a Fourier interpolation, and the curve width is proportional to the computed phonon linewidth. (b) Color contour plots of the scattering function as a function of energy and \mathbf{Q} obtained using INS, theoretical q -voxel, and theoretical q -point results. The q -voxel dimensions are 0.025 reciprocal lattice units (r.l.u.) along the $[H, H, 0]$ direction (i.e., the dispersion direction) and relaxed to 0.2 r.l.u. along the orthogonal directions $[0, 0, L]$ and $[H, -H, 0]$. (c) and (d) Scattering function as a function of energy at selected Q points, corresponding to purple and black lines in the color contour plots. The red and green curves are theoretical q -voxel and q -point scattering functions, respectively; black points are INS measurements.

to the large slope in the latter case. The preceding examples already illustrate that one can only meaningfully compare theory and experiment if q -voxel quantities are being employed.

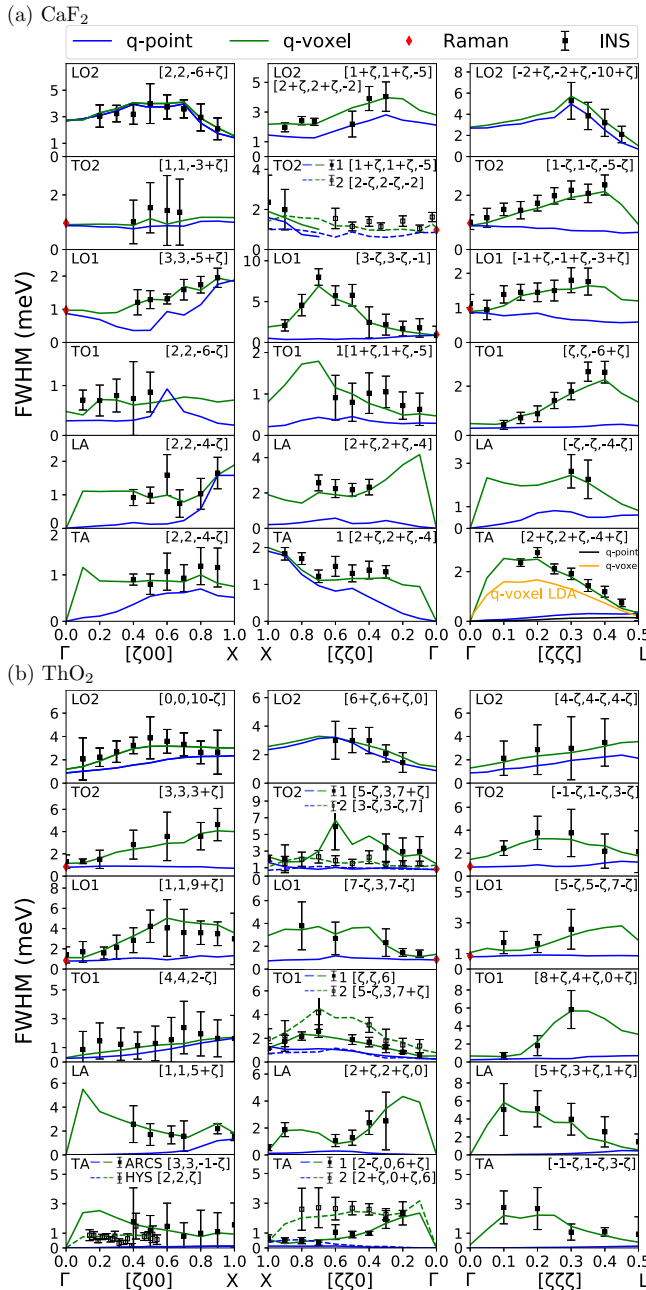


FIG. 2. FWHMs of the scattering function peaks as a function of q in various zones for CaF_2 (a) and ThO_2 (b) at $T = 300$ K. The DFT (SCAN) q -point and q -voxel results are shown as blue and green curves, respectively; INS results are shown as black points. Certain panels contain multiple modes (see legend). The q -voxel dimensions are reported in the Supplemental Material [8]. Previous Raman measurements are denoted by a red diamond [12,13].

Having illustrated that accounting for the q -voxel scattering function can be critical to describing experiments, we now proceed to comprehensively quantify the differences across the Brillouin zone for both CaF_2 and ThO_2 . In Fig. 2, we compare the full width at half maximum (FWHM) of each peak obtained from the INS q -voxel scattering function, the theoretical q -voxel scattering function, and the theoretical q -point scattering function (see Supplemental Material [8] for

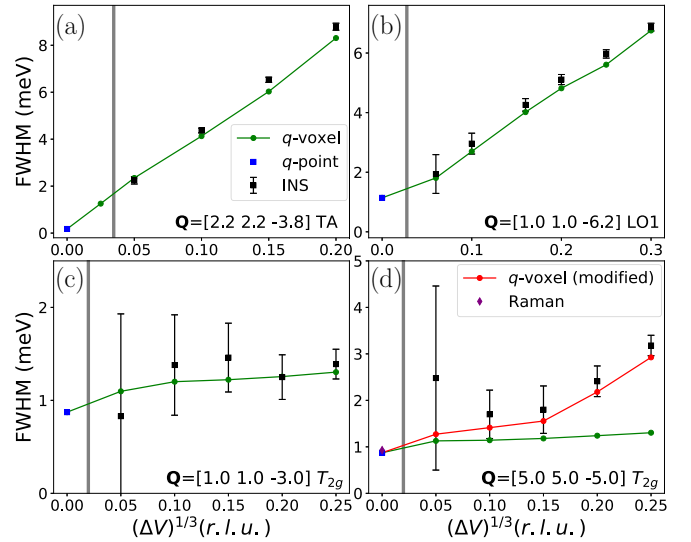


FIG. 3. The FWHM as a function of the cubic q -voxel dimension in CaF_2 at $T = 300$ K for three modes: the TA mode at $\mathbf{Q} = [2.2, 2.2, -3.8]$ (a), the LO1 mode at $\mathbf{Q} = [1.0, 1.0, -6.2]$ (b), and the T_{2g} mode at $\mathbf{Q} = [1.0, 1.0, -3.0]$ (c) and $\mathbf{Q} = [5.0, 5.0, -5.0]$ (d). See text for an explanation of the q -voxel (modified) result (red curve). The q resolution of the instrument is shown by a gray vertical line. The Raman measurement of the T_{2g} width in CaF_2 by Elliott *et al.* [12] is shown as a purple diamond.

\mathbf{Q} and voxel sizes). Following standard INS conventions, the energy resolution is removed from the INS scattering function peak width [3,14]. The INS and theoretical q -voxel FWHM results are in favorable agreement across all modes and q paths, while there is a substantial difference with the FWHM obtained from the theoretical q -point scattering function in most cases. The acoustic modes, which are highly relevant for thermal conductivity, show a strong difference between q -voxel and q -point FWHM values. We also compare our theoretical results at the Γ point with the Raman measurements of the T_{2g} widths in CaF_2 [12] and ThO_2 [13], indicated with a red diamond, demonstrating good agreement with the q -point result, which is to be expected. In summary, we have shown that it is critical to employ the q voxel in order to validate a first-principles theory using INS.

In the preceding analysis, we demonstrated that theory and experiment are in good agreement when using the same q voxel, and that the results can be substantially different from the q -point results. Now we explore the effect of voxel size in the case of a cubic voxel and examine the possibility of extrapolating the q -voxel results to zero voxel size in order to recover the q -point results, which would allow INS experiments to independently obtain q -point peak widths. The q -voxel size used in INS data analysis is a compromise between having good counting statistics (larger volume) and minimizing contamination from neighboring regions in reciprocal space (smaller volume). The minimum possible INS q -voxel size will be set by the instrument q resolution, though this is normally far too small to obtain sufficient counting statistics. The effects of the q -voxel size on the experimental FWHM of CaF_2 is shown in Fig. 3 for three different modes: the TA mode at $\mathbf{Q} = [2.2, 2.2, -3.8]$, the LO1 mode at $\mathbf{Q} =$

$[1.0, 1.0, -6.2]$, and the T_{2g} mode (i.e., LO1+TO2) at $\mathbf{Q} = [1.0, 1.0, -3.0]$ and $\mathbf{Q} = [5.0, 5.0, -5.0]$. With the exception of the T_{2g} mode at $\mathbf{Q} = [5.0, 5.0, -5.0]$ [i.e., Fig. 3(d)], the theoretical results are in good agreement with experiment for a sufficiently large voxel size, and the exception can be attributed to the overlap of the T_{2g} peak with the TO1 peak, which corrupts the fitting process for the experimental data which must account for the energy resolution of the instrument. To make a direct comparison, we convolve the theoretical results with the energy resolution and then perform the identical fitting process used for the experimental results where the energy resolution is removed [see red curve in Fig. 3(d)]. This modified theoretical result now agrees well with experiment for large q -voxel sizes and recovers the usual theoretical q -voxel results at small q -voxel sizes. Our analysis resolves a previous anomaly in the literature, explaining why the INS peak width of the T_{2g} mode was found to be more than twice that of Raman measurements [15]. Nonetheless, the simplest solution to this problem is to choose a more favorable zone, as shown in Fig. 3(c). In all the preceding examples, we see that sufficiently small voxel sizes lead to poor results for the experimental case given the poor counting statistics, as expected. Furthermore, it appears that there is sufficient uncertainty within the experimental measurements which would preclude the possibility of extrapolating to zero voxel size to obtain the peak width purely from experiment. The effects on noncubic voxels are explored in Sec. VII of the Supplemental Material [8].

We have demonstrated that the q -voxel peak widths from theory and experiment are in good agreement at room temperature. This agreement serves as a verification of the quality of our cubic phonon interactions, in addition to the level of perturbation theory used to construct the scattering function. The former is an indirect assessment of the quality of the approximation to the exchange-correlation energy used within DFT, and it should be emphasized that the SCAN functional is critical to such good agreement, whereas the local density approximation (LDA) [21] produces substantial deviations (see Fig. 2(a), orange curve, and the Supplemental Material [8], Sec. VIII). We can now predict other quantities, such as thermal conductivity, and anticipate robust results. The thermal conductivity can be computed by solving the linearized Boltzmann transport equation (LBTE) [22–24]. Within the relaxation time approximation (RTA), the LBTE solution is obtained as an explicit function of the phonon spectrum and the phonon linewidths. The RTA is sometimes an excellent approximation to the LBTE solution, and previous work has demonstrated that this is the case in CaF_2 [25]; we reach the same conclusion in both CaF_2 and ThO_2 . Therefore we expect our predicted thermal conductivity to be very robust, and we evaluate both CaF_2 and ThO_2 .

In the case of CaF_2 [Fig. 4(a)], our predictions are in good agreement with all available experimental data [16–18] in the temperature range 200–300 K. At low temperatures, the results of both Slack [16] and Popov *et al.* [18] are somewhat higher than our predictions, though the single measurement at $T = 77$ K by Eucken [17] is below our result. In the case of ThO_2 [Fig. 4(b)], our predicted thermal conductivity is in good agreement with the data of Bakker *et al.* [20], which extend from 300 to 450 K, and reasonable comparison is

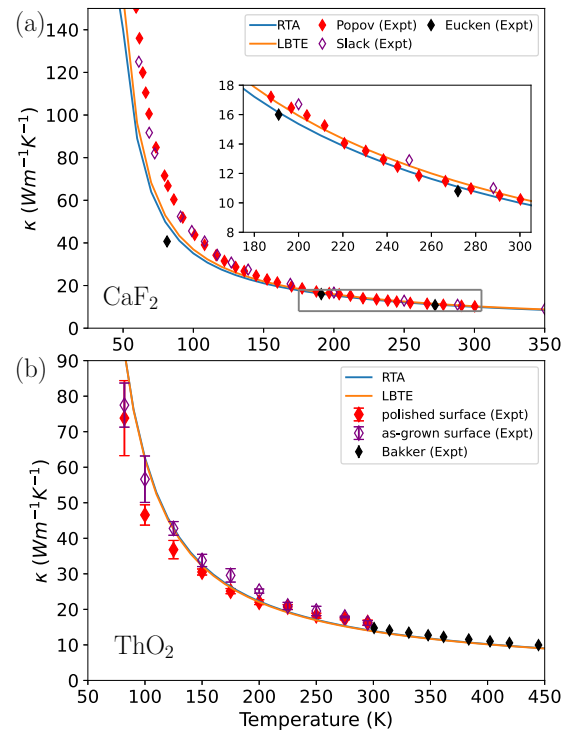


FIG. 4. Thermal conductivity κ as a function of temperature in CaF_2 (a) and ThO_2 (b). Our DFT (SCAN) results are denoted with orange and blue curves for LBTE and RTA solutions, respectively. Experimental measurements in CaF_2 by Slack [16], Eucken [17], and Popov *et al.* [18,19] are shown, in addition to measurements in ThO_2 by Bakker *et al.* [20] and our own measurements (with one sample having a polished surface [8]).

found with our measurements from 82 to 295 K. The higher conductivity predicted at low temperatures as compared with our experiments may be due to small, native impurity concentrations resulting from the hydrothermal growth process. Our laser-based measurements show nontrivial variability at low temperatures based on the surface condition of the sample, and there is a small difference with the data of Bakker *et al.* near room temperature. It is difficult to assess which experimental results are more reliable. Comparison with previous first-principles calculations is provided in the Supplemental Material for both CaF_2 and ThO_2 [8].

In summary, we have shown that the q voxel of the INS-measured scattering function must be accounted for when comparing with theoretical predictions, elucidating why INS peak widths had not been well matched to predictions until now. Given that the q voxel can be straightforwardly implemented within theory, INS is thus elevated to a refined judge of all ingredients of a quasiparticle theory of phonons, whether *ab initio* or empirical. The q voxel should be carefully considered in the design of future INS instruments, with the possible goal of allowing INS to independently extrapolate to the q -point limit.

The U.S. Department of Energy (DOE) will provide public access to these results of federally sponsored research in accordance with the DOE Public Access Plan [26].

INS measurements, first-principles calculations, crystal growth, and thermal conductivity measurements were supported by the Center for Thermal Energy Transport under Irradiation, an Energy Frontier Research Center funded by the U.S. Department of Energy (DOE) Office of Science, Office of Basic Energy Sciences. Neutron scattering data acquisition and provision of CaF₂ were supported by the U.S. DOE Office of Science, Basic Energy Sciences, Materials Science and Engineering Division. Portions of this research used resources at the Spallation Neutron Source, a U.S. DOE Office of Science User Facility operated by the Oak Ridge National Laboratory. This research used resources of the National Energy Research Scientific Computing Center, a DOE Office of Science User Facility supported by the Office of Science of the U.S. Department of Energy under Contract No. DE-AC02-05CH11231. The formulation and encoding of linewidths via irreducible derivatives was supported by Grant No. DE-

SC0016507 funded by the U.S. Department of Energy, Office of Science. ORNL is managed by UT-Battelle, LLC, under Contract No. DE-AC05-00OR22725 for the U.S. Department of Energy. The U.S. Government retains, and the publisher, by accepting the article for publication, acknowledges that the U.S. Government retains a nonexclusive, paid-up, irrevocable, worldwide license to publish or reproduce the published form of this manuscript, or allow others to do so, for U.S. Government purposes.

M.S.B., H.M., and M.E.M. performed INS measurements; E.X., L.F., and C.A.M. performed first-principles calculations; J.M.M. performed crystal growth measurements; C.A.D., A.R.K., and D.H.H. performed thermal conductivity measurements; R.P.H. acquired the neutron scattering data and provided the CaF₂; and L.F. and C.A.M. formulated and encoded the linewidths via irreducible derivatives.

-
- [1] D. S. Kim, O. Hellman, N. Shulumba, C. N. Saunders, J. Y. Lin, H. L. Smith, J. Herriman, J. L. Niedziela, D. L. Abernathy, C. W. Li, and B. Fultz, *Phys. Rev. B* **102**, 174311 (2020).
- [2] A. Glensk, B. Grabowski, T. Hickel, J. Neugebauer, J. Neuhaus, K. Hradil, W. Petry, and M. Leitner, *Phys. Rev. Lett.* **123**, 235501 (2019).
- [3] D. L. Abernathy, M. B. Stone, M. Loguillo, M. Lucas, O. Delaire, X. Tang, J. Lin, and B. Fultz, *Rev. Sci. Instrum.* **83**, 015114 (2012).
- [4] S. Shapiro, I. Zaliznyak, L. Passell, V. Ghosh, W. Leonhardt, and M. Hagen, *Phys. B: Condens. Matter* **385-386**, 1107 (2006).
- [5] C. A. Dennett, W. R. Deskins, M. Khafizov, Z. Hua, A. Khanolkar, K. Bawane, L. Fu, J. M. Mann, C. A. Marianetti, L. He, D. H. Hurley, and A. El-Azab, *Acta Mater.* **213**, 116934 (2021).
- [6] J. Sun, A. Ruzsinszky, and J. Perdew, *Phys. Rev. Lett.* **115**, 036402 (2015).
- [7] L. Fu, M. Kornbluth, Z. Cheng, and C. A. Marianetti, *Phys. Rev. B* **100**, 014303 (2019).
- [8] See Supplemental Material at <http://link.aps.org/supplemental/10.1103/PhysRevB.106.144310> for details of sample preparation, INS information, and details of DFT calculations. References [3–7,10,14,18,19,21,25,27–40] are cited.
- [9] J. J. Kokkedee, *Physica (Amsterdam)* **28**, 374 (1962).
- [10] A. Maradudin and A. Fein, *Phys. Rev.* **128**, 2589 (1962).
- [11] G. Shirane, S. M. Shapiro, and J. M. Tranquada, *Neutron Scattering with a Triple-Axis Spectrometer: Basic Techniques* (Cambridge University Press, Cambridge, 2002).
- [12] R. J. Elliott, W. Hayes, W. G. Kleppmann, A. J. Rushworth, and J. F. Ryan, *Proc. R. Soc. London, Ser. A* **360**, 317 (1978).
- [13] R. Rao, R. Bhagat, N. P. Salke, and A. Kumar, *Appl. Spectrosc.* **68**, 44 (2014).
- [14] S. D. Bruce, J. Higinbotham, I. Marshall, and P. H. Beswick, *J. Magn. Reson.* **142**, 57 (2000).
- [15] K. Schmalzl, D. Strauch, and H. Schober, *Phys. Rev. B* **68**, 144301 (2003).
- [16] G. A. Slack, *Phys. Rev.* **122**, 1451 (1961).
- [17] A. Eucken, *Ann. Phys. (Berlin)* **339**, 185 (1911).
- [18] P. A. Popov, P. P. Fedorov, and V. V. Osiko, *Dokl. Phys.* **59**, 199 (2014).
- [19] The experimental data of Popov *et al.* [18] were digitized incorrectly by Qi *et al.* [25].
- [20] K. Bakker, E. H. P. Cordfunke, R. J. M. Konings, and R. P. C. Schram, *J. Nucl. Mater.* **250**, 1 (1997).
- [21] J. P. Perdew and A. Zunger, *Phys. Rev. B* **23**, 5048 (1981).
- [22] D. A. Broido, A. Ward, and N. Mingo, *Phys. Rev. B* **72**, 014308 (2005).
- [23] D. A. Broido, L. Lindsay, and A. Ward, *Phys. Rev. B* **86**, 115203 (2012).
- [24] L. Chaput, *Phys. Rev. Lett.* **110**, 265506 (2013).
- [25] Y.-Y. Qi, T. Zhang, Y. Cheng, X.-R. Chen, D.-Q. Wei, and L.-C. Cai, *J. Appl. Phys.* **119**, 095103 (2016).
- [26] <http://energy.gov/downloads/doe-public-access-plan>.
- [27] M. Mann, D. Thompson, K. Serivalsatit, T. M. Tritt, J. Ballato, and J. Kolis, *Cryst. Growth Des.* **10**, 2146 (2010).
- [28] M. S. Bryan, L. Fu, K. Rickert, D. Turner, T. A. Prusnick, J. M. Mann, D. L. Abernathy, C. A. Marianetti, and M. E. Manley, *Commun. Phys.* **3**, 217 (2020).
- [29] J. Y. Lin, A. Banerjee, F. Islam, M. D. Le, and D. L. Abernathy, *Phys. B (Amsterdam)* **562**, 26 (2019).
- [30] M. B. Stone, J. L. Niedziela, D. L. Abernathy, L. DeBeer-Schmitt, G. Ehlers, O. Garlea, G. E. Granroth, M. Graves-Brook, A. I. Kolesnikov, A. Podlesnyak, and B. Winn, *Rev. Sci. Instrum.* **85**, 045113 (2014).
- [31] C. A. Dennett, Z. Hua, A. Khanolkar, T. Yao, P. K. Morgan, T. A. Prusnick, N. Poudel, A. French, K. Gofryk, L. He, L. Shao, M. Khafizov, D. B. Turner, J. M. Mann, and D. H. Hurley, *APL Mater.* **8**, 111103 (2020).
- [32] P. E. Blöchl, O. Jepsen, and O. K. Andersen, *Phys. Rev. B* **49**, 16223 (1994).
- [33] G. Kresse and D. Joubert, *Phys. Rev. B* **59**, 1758 (1999).
- [34] A. C. Momin, E. B. Mirza, and M. D. Mathews, *J. Nucl. Mater.* **185**, 308 (1991).
- [35] B. Schumann and H. Neumann, *Cryst. Res. Technol.* **19**, K13 (1984).
- [36] H. Nakamura and M. Machida, *J. Nucl. Mater.* **519**, 45 (2019).
- [37] R. Bader, M. Brehm, R. Ebner, H. Heller, L. Palm, and F.

- Wagner, *High Performance Computing in Science and Engineering, Munich 2002*, edited by S. Wagner, A. Bode, W. Hanke, and F. Durst (Springer, Berlin, 2003).
- [38] R. M. Hazen and L. W. Finger, *J. Appl. Crystallogr.* **14**, 234 (1981).
- [39] O. Arnold, J. Bilheux, J. Borreguero, A. Buts, S. Campbell, L. Chapon, M. Doucet, N. Draper, R. Ferraz Leal, M. Gigg, V. Lynch, A. Markvardsen, D. Mikkelsen, R. Mikkelsen, R. Miller, K. Palmen, P. Parker, G. Passos, T. Perring, P. Peterson *et al.*, *Nucl. Instrum. Methods Phys. Res., Sect. A* **764**, 156 (2014).
- [40] F. Akeroyd, S. Ansell, S. Antony, O. Arnold, A. Bekasovs, J. Bilheux, J. Borreguero, K. Brown, A. Buts, S. Campbell, D. Champion, L. Chapon, M. Clarke, S. Cottrell, R. Dalglish, D. Dillow, M. Doucet, N. Draper, R. Fowler, M. A. Gigg *et al.* (Mantid Project), Mantid: Manipulation and Analysis Toolkit for Instrument Data, 2013, <http://dx.doi.org/10.5286/SOFTWARE/MANTID>.